Electronic Supplementary Material (ESI) for Journal of Materials Chemistry A.

Supplementary materials for

Self-assembly of heterogeneous microreactor with carbon dots embedded in Ti-MOF derived $ZnIn_2S_4/TiO_2$ microcapsule for efficient CO_2 photoreduction

Dongxue Wu[a], Qian Liang[a,*], Honglin Si[b], Xiong Yan[b], Hui Huang[b], Zhongyu Li[a,*] and Zhenhui Kang[b,c,d,*]

[a]Jiangsu Key Laboratory of Advanced Catalytic Materials and Technology, School of Petrochemical Engineering, Changzhou University, Changzhou 213164, China. E-mail: qianliang@cczu.edu.cn; zhongyuli@mail.tsinghua.edu.cn

[b]Institute of Functional Nano and Soft Materials Laboratory (FUNSOM), Jiangsu Key Laboratory for Carbon-Based Functional Materials & Devices, Soochow University, Suzhou 215123, China. E-mail: zhkang@suda.edu.cn

[c]Macao Institute of Materials Science and Engineering, Macau University of Science and Technology, Taipa, 999078, Macau SAR, China. E-mail: zhkang@must.edu.mo

[d] Institute of Advanced Materials, Northeast Normal University, Changchun, 130024, China. E-mail: kangzh@nenu.edu.cn

Supplementary Text

1. Experimental section

1.1 Material

All reagents were commercial materials of reagent grade and used without further purification. Zinc chloride ($ZnCl_2$), thioacetamide (TAA), methanol, ethanol, indium chloride tetrahydrate ($InCl_3 \cdot 4H_2O$), N, N-dimethylformamide (DMF), tetrabutyl titanate $Ti(OC_4H_9)_4$ and 2-Aminoterephthalic acid (NH_2-BDC) were purchased from Sinopharm Chemical Reagent Co., Ltd. (Shanghai, China).

1.2 Synthesis.

1.2.1 Synthesis of CDs.

The CDs were prepared by a typical electrochemical method [1]. In general, two graphite rods after ultrasonic cleaning were inserted into deionized (DI) water as anode and cathode respectively, and then a 30 V bias was applied between the two electrodes using a direct current power supply. Continue stirring until the stone grinding rod was gradually corroded and the colorless electrolyte turned into a dark solution. The obtained dark solution was filtered and collected by centrifugation, and then freeze-dried to obtain CDs powder. Finally, the CDs powder was dispersed in DI water (0.7 mg mL^{-1}).

1.2.2 Synthesis of NH_2-MIL-125(Ti)

NH_2-MIL-125(Ti) was prepared according to the previous literature [2]. In a typical synthesis, $Ti(OC_4H_9)_4$ (0.52 mL, 1.5 mmol) and NH_2-H_2BDC (1.087 g, 6.0 mmol) were added into a mixed solution containing DMF and MeOH (24.3 mL: 2.7 mL). And the mixture solution was further stirred for 30 min at room temperature to form a uniform and stable solution. Subsequently, the solution was sealed in a 100 mL Teflon-lined autoclave and maintained at 150°C for 24 h. The resulting mixture was cooled to room temperature and a yellow powder was obtained by centrifugation, and washed using DMF and methanol for several times to remove unreacted organic linkers, Finally, the product was dried at 60°C under vacuum for 12 h.

1.3 The experimental method of transient photovoltage (TPV).

The TPV measurements were conducted on films samples (1.5 cm × 4 cm) deposited on indium-tin oxide (ITO) glass substrates at room temperature. A 10 mg mL^{-1} sample aqueous solution was dripped on the ITO substrate, and then dried in air to obtain the films samples. The working electrode (ITO glass modified with samples) and the counter electrode (Pt wire) were wetted with N_2 or O_2-saturated acetonitrile and N_2-saturated acetonitrile/water aqueous (0.5 vol%). Meanwhile, we also measured the powder samples, which were covered on the Pt network (1 cm × 1 cm). The samples were excited by a third-harmonic Nd: YAG laser (Polaris II, New Wave Research, Inc.) with a laser radiation pulse (wavelength 355 nm, pulse width 5 ns).

1.4 Characterizations

The crystal structures and crystallinity of microreactors were analyzed by powder X-ray diffractometer (Bruker D8 Advance) with Cu Kα radiation. The morphologies and microstructures of microreactors were measured on field-emission scanning electron microscopy (FE-SEM, Hitachi) as well as transmission electron microscopy (TEM, JEOL 2100). Fourier transform infrared spectroscopy (FT-IR) spectra were performed on the EQUI-NOX55 (Germany Bruker). N_2 adsorption-desorption curves were obtained on Micromeritics ASAP 2000 to analyze porous structure. The optical properties of microreactors were performed on UV-vis diffuse reflectance spectroscopy (DRS) with a Shimadzu UV-3600 UV-vis spectrophotometer. The steady-state photoluminescence (PL) spectra were recorded on a Cary Eclipse fluorescence spectrophotometer. Time-resolved photoluminescence (TR-PL) decay spectra were measured on an FLS1000 at an excitation wavelength of 365 nm. The chemical composition and state were investigated by X-ray photoelectron spectra (XPS) applied on a Thermo ESCALAB 250 spectrometer with an Al Kα X ray source. *In-situ* FT-IR spectra were acquired by the Bruker INVENIO R FT-IR spectrometer equipped with an *in situ* diffuse reflectance cell (Harrick) to study the CO_2 photoreduction process.

1.5 Photocatalytic CO_2 reduction

The photocatalytic CO_2 reduction was tested in a 200 mL Pyrex glass reactor, and 10 mg photocatalysts were dispersed in H_2O/ethyl acetate (EA). After complete evacuation of the reaction system, high-purity CO_2 gas was injected into the airtight system. The reaction system was cooled by circulating water to weaken the heating effect and decrease the solvent evaporation. A 300 W xenon lamp was assembled with the AM 1.5G filter simulated solar illumination (Beijing China Education Aulight Co., Ltd.). The illumination distance was settled on 6 cm from the sample. The gaseous products were analyzed by gas chromatography (GC-7860 Plus) equipped with FID. The cycling experiments of as-prepared samples were conducted as follows: after the reaction, the photocatalyst was separated from the solution, rinsed with deionized water, and dried at 60°C for the next run.

1.6 Photoelectrochemical measurement

Photoelectrochemical properties of catalysts were measured on a CHI660D electrochemical analyzer with the conventional three-electrode cell, including platinum wire as the counter electrode, Ag/AgCl as the reference electrode, and working electrode. 0.5 M Na_2SO_4 solution was used as the electrolyte. The working electrode was prepared as follows: 2 mg of as-prepared sample was dispersed in 2 mL of ethanol with 75 μL of Nafion. Then, the above suspension (100 μL) was dropped onto the FTO glass and then dried at 60°C. Under a 300 W xenon lamp with AM 1.5G filter, the electrochemical impedance spectroscopy (EIS) and transient photocurrent response were obtained. The Mott-Schottky curves of samples were obtained by varying the frequencies.

Supplementary Figures

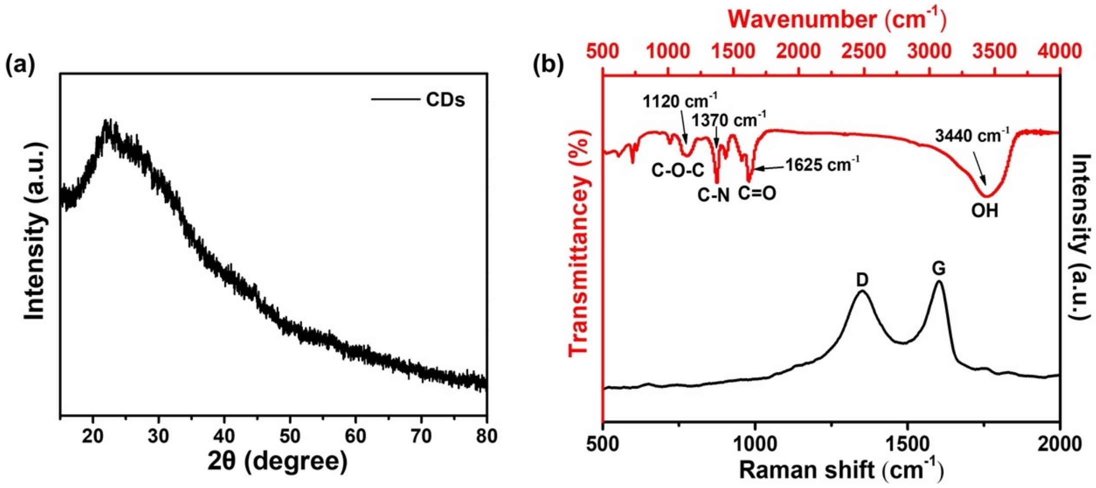

Fig. S1 (a) XRD pattern, (b) Raman and FT-IR spectra of CDs.

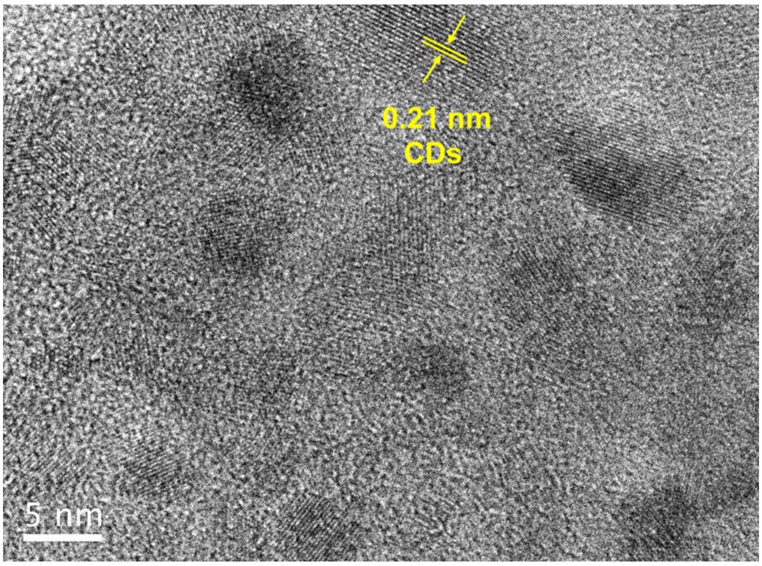

Fig. S2 HRTEM image of CDs.

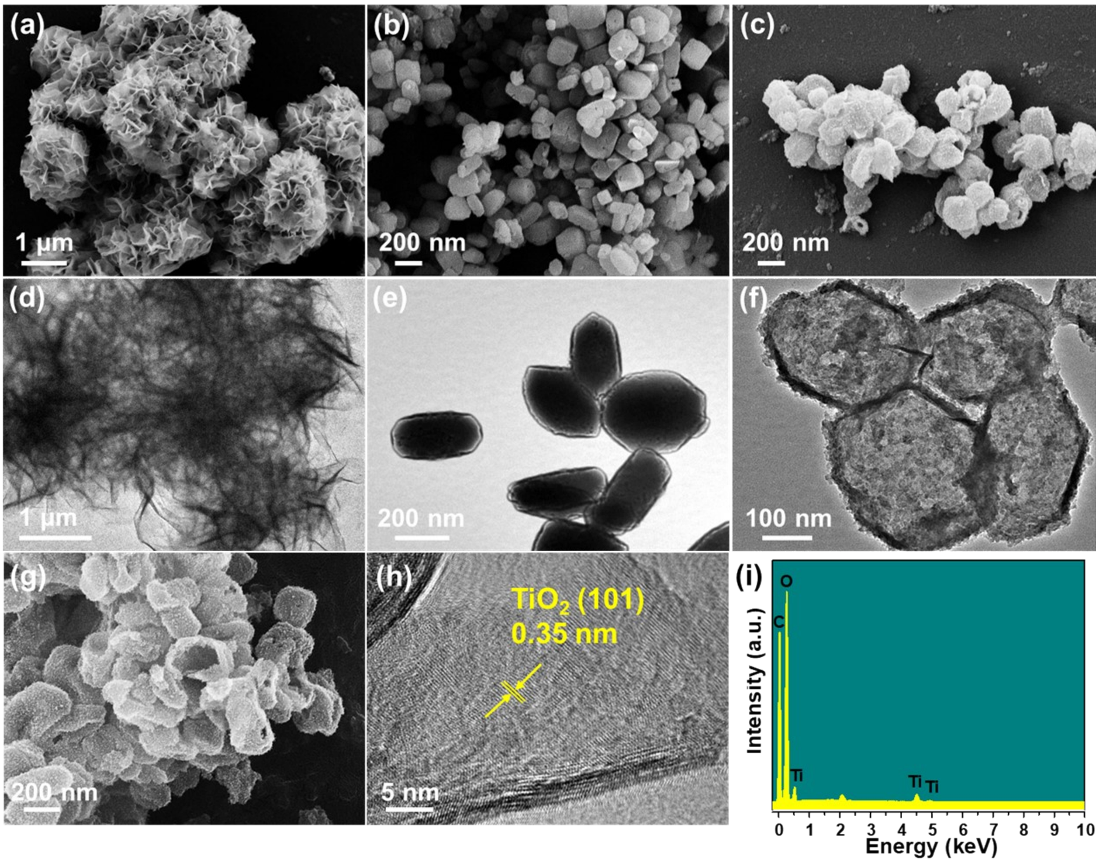

Fig. S3 SEM images of (a) $ZnIn_2S_4$, (b) NH_2-MIL-125 and (c) ZIS(60)/TiO_2. TEM images of (d) $ZnIn_2S_4$, (e) NH_2-MIL-125 and (f) ZIS(60)/TiO_2. (g) SEM image, (h) HRTEM image and (i) EDS pattern of m-TiO_2.

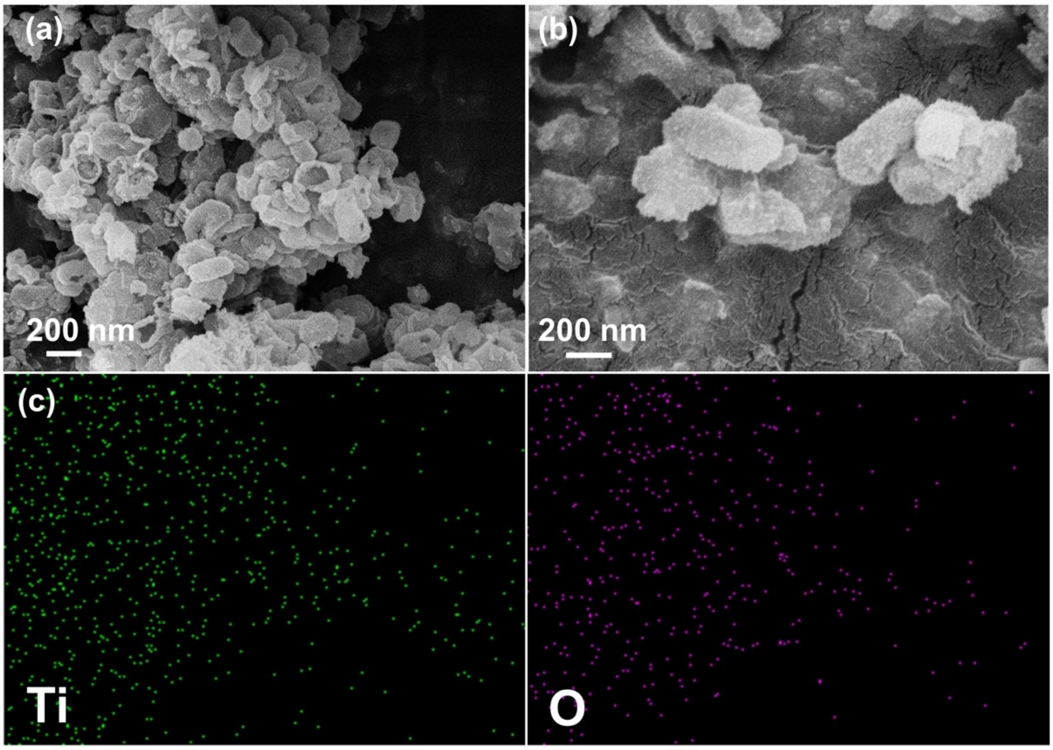

Fig. S4 (a, b) SEM images and (c) EDS mapping images of m-TiO_2.

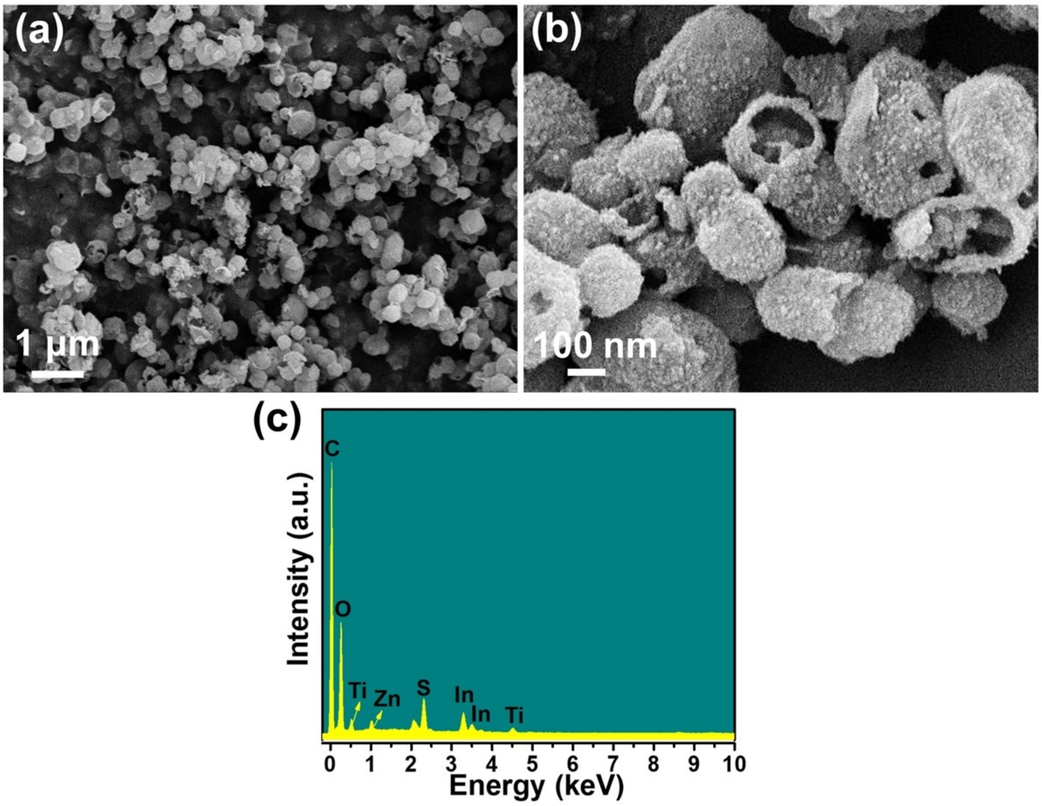

Fig. S5 (a, b) SEM images and (c) EDS pattern of 5-CDs/ZIS/TiO_2.

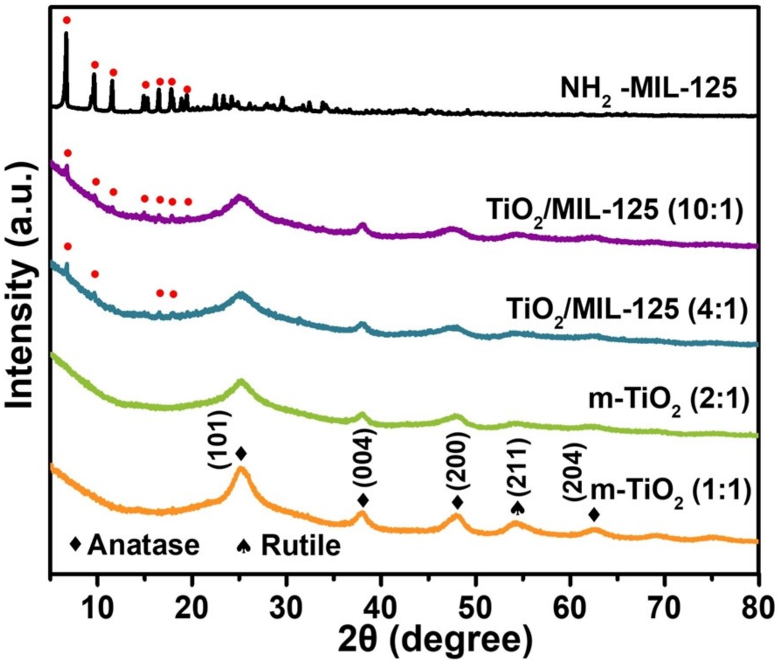

Fig. S6 XRD patterns of pristine NH$_2$-MIL-125, TiO$_2$/MIL-125 and m-TiO$_2$ composites with the weight ratios of NH$_2$-MIL-125 : TAA.

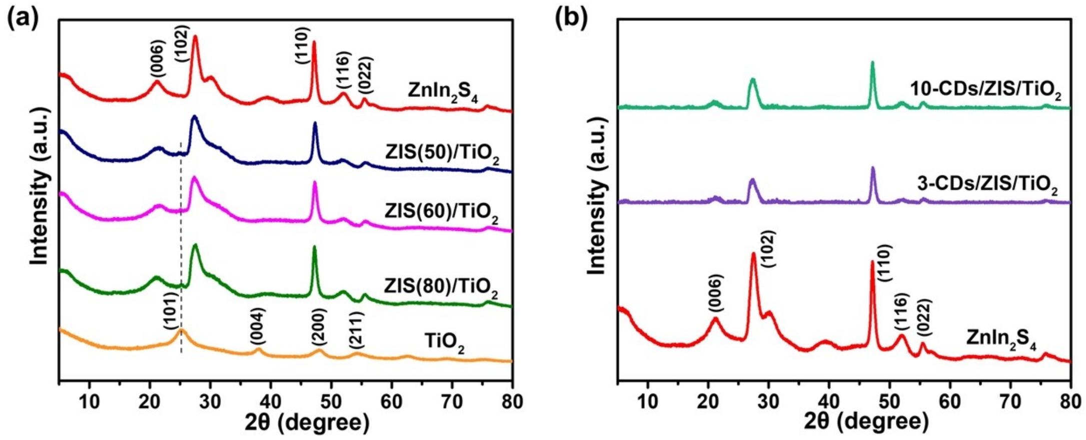

Fig. S7 (a) XRD patterns of $ZnIn_2S_4$, m-TiO_2, ZIS(50)/TiO_2, ZIS(60)/TiO_2, and ZIS(80)/TiO_2. (b) XRD patterns of $ZnIn_2S_4$, CDs/ZIS/TiO_2 composites with different CDs loading.

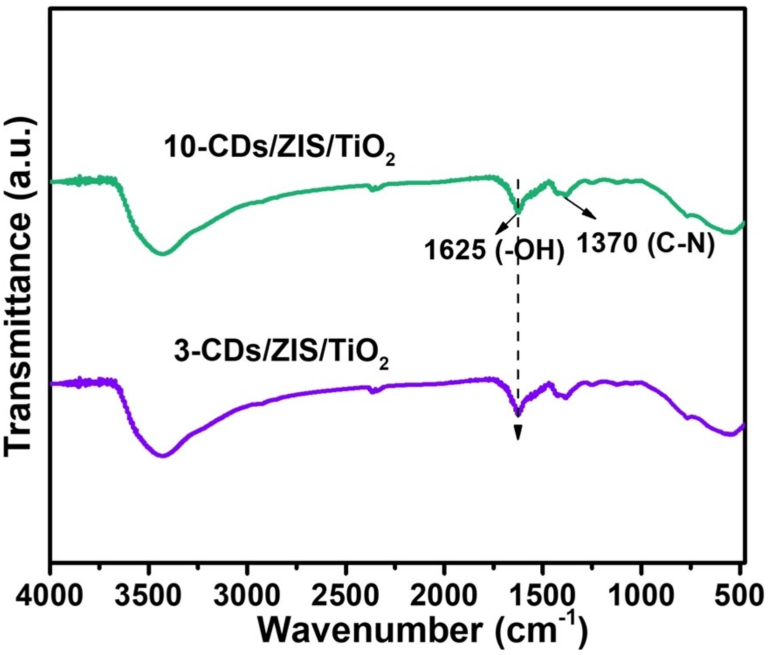

Fig. S8 FT-IR spectra of CDs/ZIS/TiO$_2$ composites with different CDs loading.

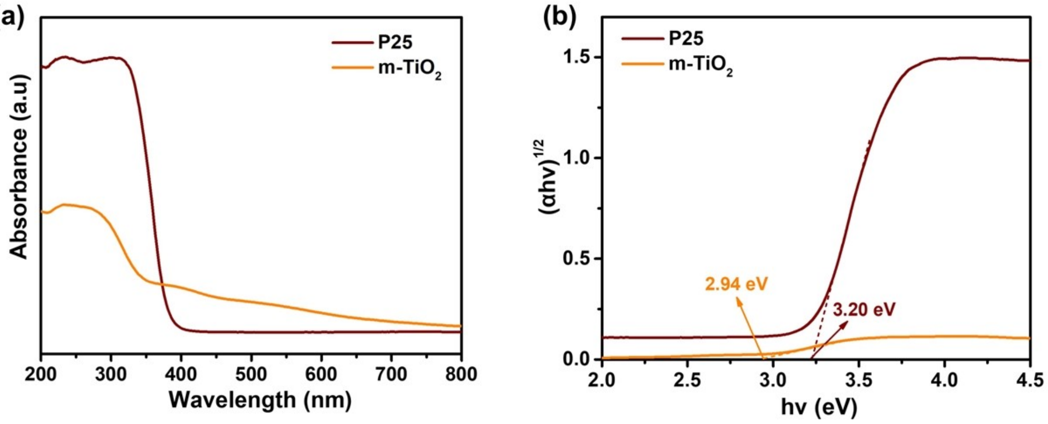

Fig. S9 (a) UV-vis spectra of P25 and m-TiO_2. (b) Tauc plots of P25 and m-TiO_2.

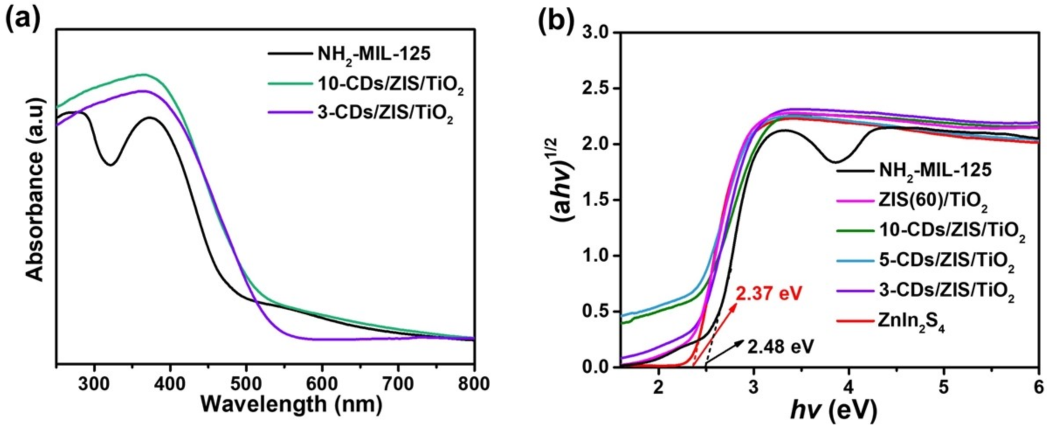

Fig. S10 (a) UV-vis spectra of NH$_2$-MIL-125, 3-CDs/ZIS/TiO$_2$, 10-CDs/ZIS/TiO$_2$ and (b) Tauc plots of NH$_2$-MIL-125 and ZnIn$_2$S$_4$.

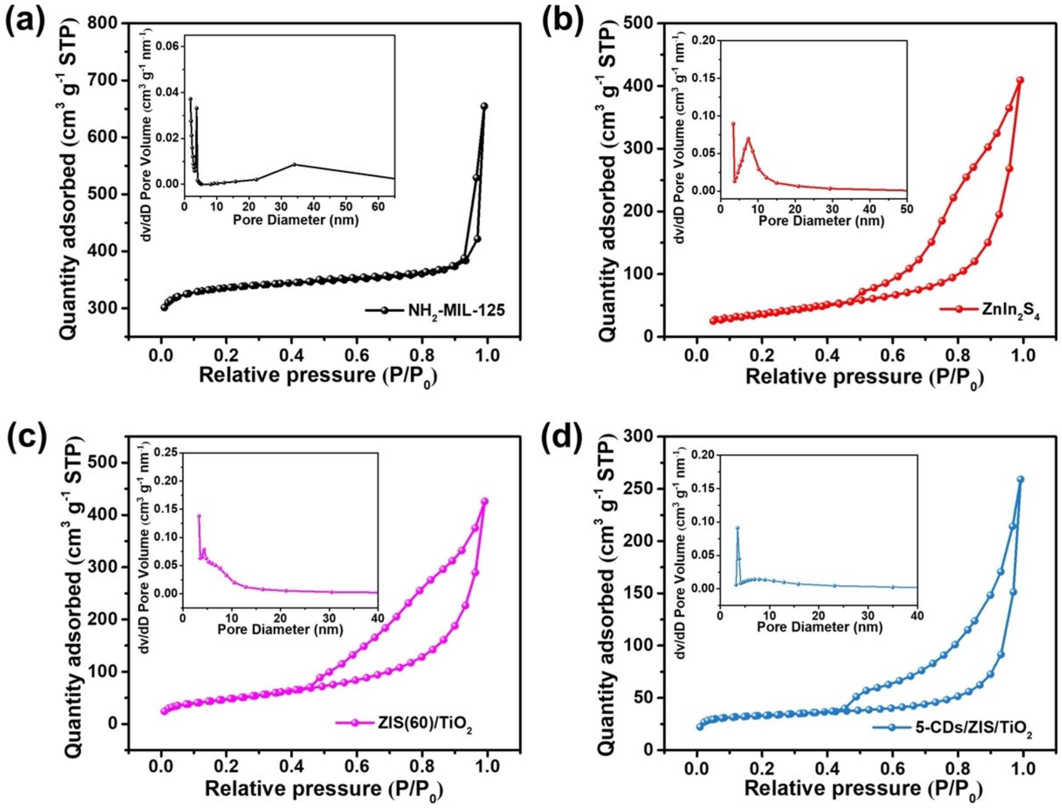

Fig. S11 N_2 adsorption-desorption isotherms of (a) NH_2-MIL-125, (b) $ZnIn_2S_4$, (c) ZIS(60)/TiO_2 and (d) 5-CDs/ZIS/TiO_2.

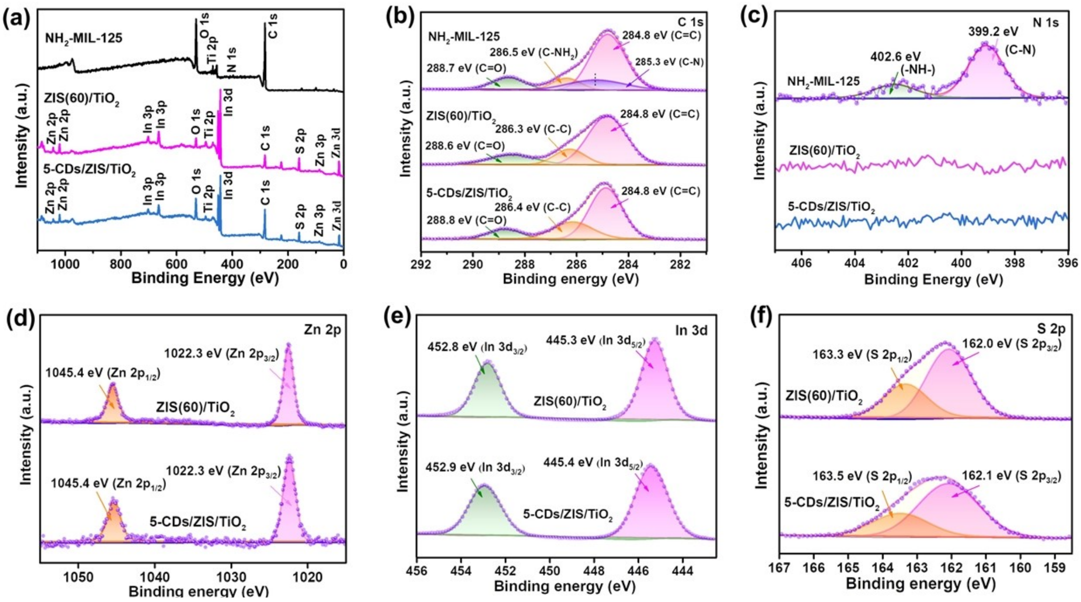

Fig. S12 (a) XPS survey spectra of NH_2-MIL-125, ZIS(60)/TiO_2 and 5-CDs/ZIS/TiO_2. High-resolution XPS spectra of NH_2-MIL-125, ZIS(60)/TiO_2 and 5-CDs/ZIS/TiO_2: (b) C 1s, (c) N 1s, (d) Zn 2p, (e) In 3d and (f) S 2p.

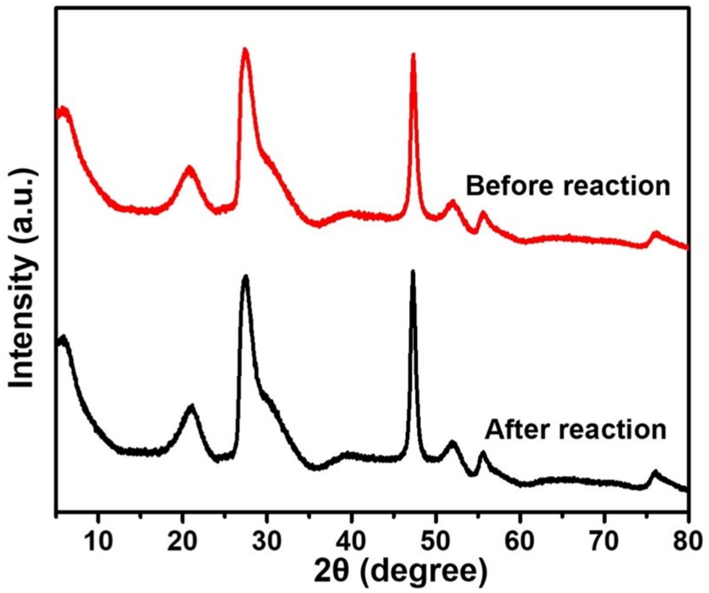

Fig. S13 XRD patterns of 5-CDs/ZIS/TiO_2 composite before and after the photocatalytic reaction.

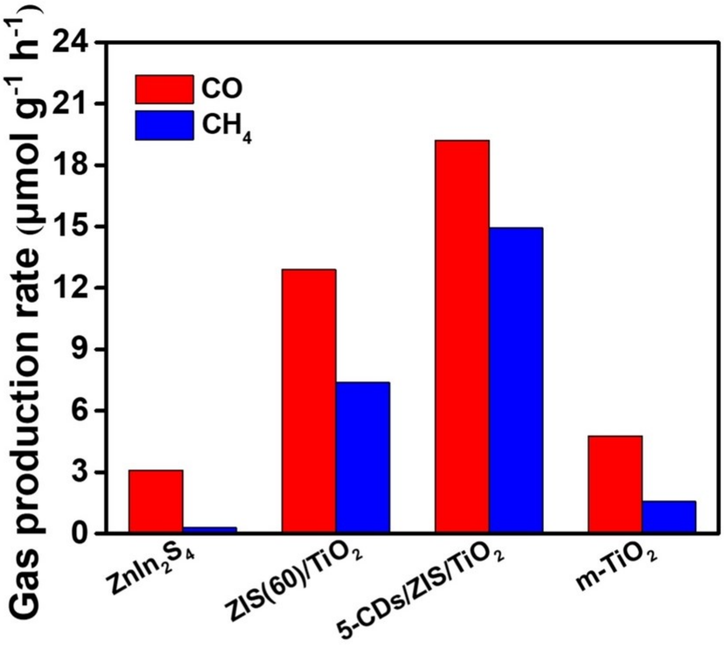

Fig. S14 Photocatalytic CO_2 reduction performances of different catalysts.

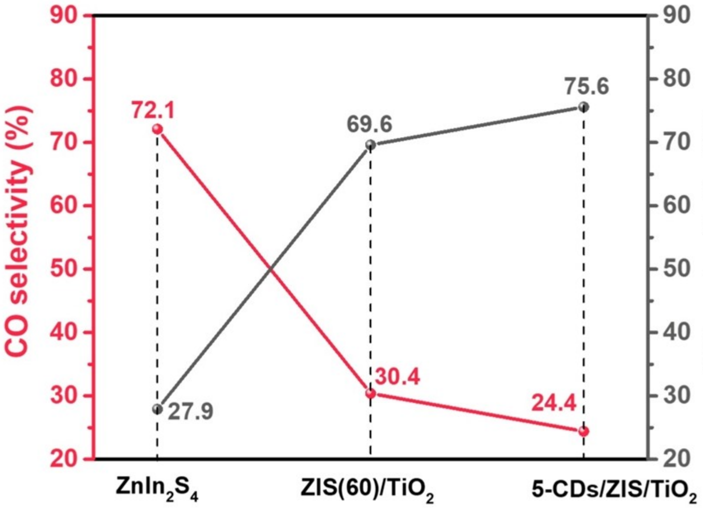

Fig. S15 The carbon products selectivity of $ZnIn_2S_4$, ZIS(60)/TiO_2 and 5-CDs/ZIS/TiO_2.

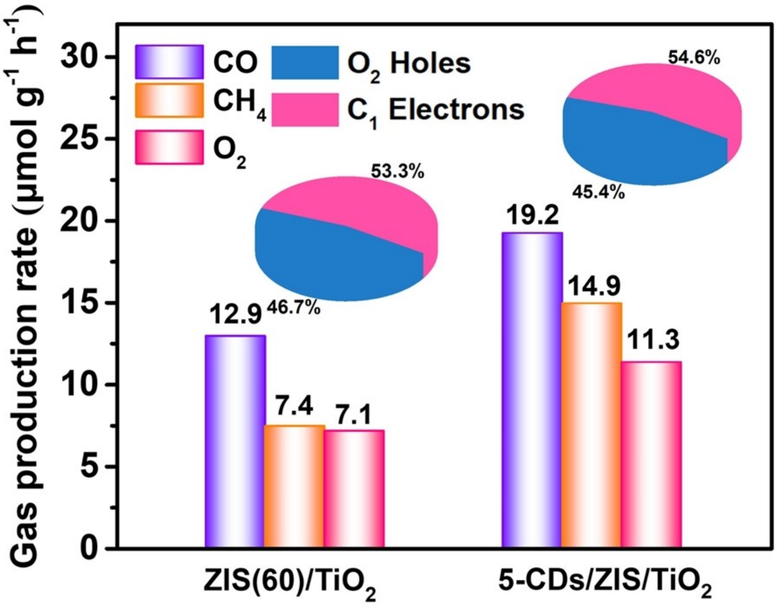

Fig. S16 Average gas evolution of oxygen and C_1 products at ZIS(60)/TiO_2 and 5-CDs/ZIS/TiO_2. The inserted pie charts are the total utilization of electrons by O_2 and C_1 evolution, indicating that the total number of reactive electrons of C_1 and reactive holes of O_2 is roughly the same.

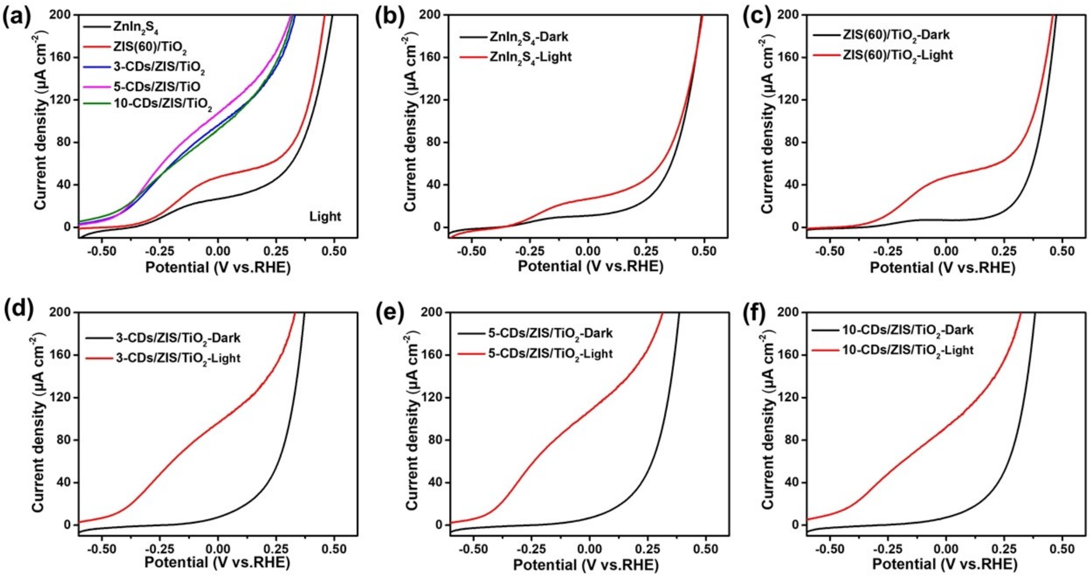

Fig. S17 Polarization curves for ZnIn$_2$S$_4$, ZIS(60)/TiO$_2$ and CDs/ZIS/TiO$_2$ composites under AM1.5 G sunlight irradiation in Na$_2$SO$_4$ with a scan rate of 5 mV s^{-1}.

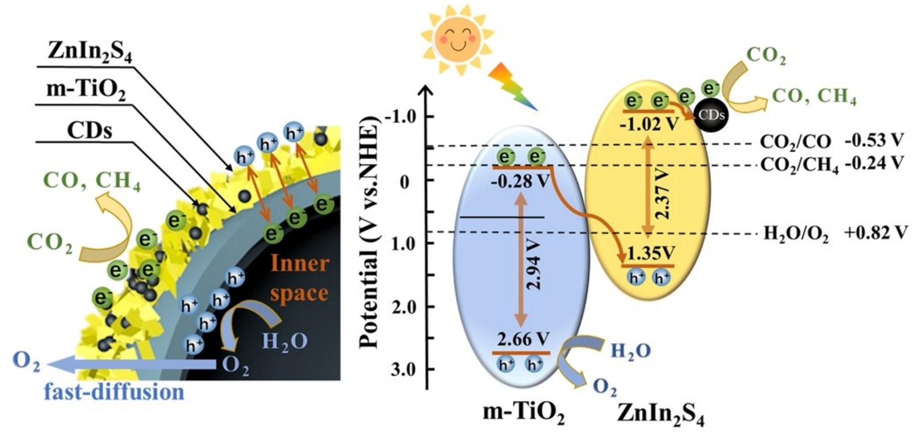

Fig. S18 Mechanism and energy band diagram of the photo-generated charge carrier transfer.

Supplementary Tables

Table S1 Porous characteristics of as-prepared samples.

Samples	S_{BET} ($m^2 \cdot g^{-1}$)	$S_{Langmuir}$ ($m^2 \cdot g^{-1}$)	Pore volume ($cm^3 \cdot g^{-1}$)	Average pore size(nm)
NH_2-MIL-125	1006	2279	0.87	19.72
$ZnIn_2S_4$	138	322	0.32	17.15
ZIS(60)/TiO_2	206	467	0.40	34.51
5-CDs/ZIS/TiO_2	272	574	0.45	14.73

Table S2 Summary of the CO and CH_4 selectivity over $ZnIn_2S_4$, m-TiO_2, ZIS(60)/TiO_2, and 5-CDs/ZIS/TiO_2.

	$ZnIn_2S_4$	ZIS(60)/TiO_2	5-CDs/ZIS/TiO_2	m-TiO_2
CO selectivity	72.1%	30.4%	24.4%	42.9%
CH_4 selectivity	27.9%	69.6%	75.6%	57.1%

Table S3 The charge transfer kinetics parameter on the interfaces of the photocatalysts based on TPV analysis.

Parameter	m-TiO$_2$	ZnIn$_2$S$_4$	ZIS(60)/TiO$_2$	5-CDs/ZIS/TiO$_2$
Attenuation constants τ (ms)	0.682	0.609	0.544	0.421
Shadow part A	0.192	0.0511	0.0341	0.0934

Table S4 The average recombination lifetime of ZnIn$_2$S$_4$ under CO$_2$-saturated MeCN and 0.5 vol% H$_2$O/MeCN (v/v)

Sample	C_1	τ_1/**ms**	C_2	τ_2/**ms**	τ_{avg}/**ms**
ZnIn$_2$S$_4$/CO$_2$	0.804	0.055	0.065	0.412	0.190
ZnIn$_2$S$_4$/H$_2$O	**0.654**	**0.410**	**0.530**	**0.561**	**0.490**

Calculation process of average recombination lifetime (τ_{avg}) in TPV curves.

Single exponential fit of time decay constant:

$$y = C_1 \cdot exp\left(-\frac{x - x_0}{\tau_1}\right) + y_0 \qquad (1)$$

C_1 is the fitting undetermined coefficient, τ_1 is time decay constant in charge recombination process, y_0 is constant term.

The formula for calculating average recombination lifetime:

$$\tau_{avg} = \frac{C_1\tau_1^2 + C_2\tau_2^2}{C_1\tau_1 + C_2\tau_2} \qquad (2)$$

According to equation (1) and (2), the calculation results are shown in Table S2:

Table S5 Comparison of similar photocatalytic systems for CO_2 reduction performance presented in recent papers.

Photocatalysts	Photosensitizer/ Sacrificial agent	Solvent	Product	Production rate/μmol g^{-1} h^{-1}	Light source	References
5-CDs/ZIS/TiO_2	/	EA/H_2O	CO **CH_4**	19.18 **13.93**	300 W Xe lamp AM 1.5G filter	**This work**
ZIS(60)/TiO	/	EA/H_2O	CO CH_4	14.01 9.62	300 W Xe lamp AM 1.5G filter	This work
$ZnIn_2S_4/TiO_2$ nanobelts	/	H_2O	CH_4	1.135	300 W Xe lamp	[3]
$ZnIn_2S_4$/N-graphene	/	H_2O	CO CH_3OH CH_4	2.45 1.37 1.01	300 W Xe lamp	[4]
$TiO_2@ZnIn_2S_4/Ti_3C_2$	/	H_2O	CO CH_4	10.17 11.33	300 W Xe lamp	[5]
$Co_9S_8@ZnIn_2S_4$/CdS	$NaSO_3$	$MeCN/H_2O$	CO H_2	82.10 1419.14	300 W Xe lamp	[6]
$C_3N_4/Au/ZnIn_2S_4$	TEOA $Co(bpy)_3^{2+}$	$MeCN/H_2O$	CO CH_4 H_2	242.3 / /	300 W Xe lamp	[7]
$ZnIn_2S_4/BiVO_4$	/	H_2O	CO CH_4	4.75 3.02	300 W Xe lamp	[8]
CeO_x-S/$ZnIn_2S_4$	TEA	$MeCN/H_2O$	CO H_2	1800 /	455 nm LEDs	[9]
0xygen-doped $ZnIn_2S_4$	TEOA $Co(bpy)_3^{2+}$	$MeCN/H_2O$	CO H_2	1680 /	λ ≥ 420 nm	[10]
$ZnIn_2S_4$/g-C_3N_4	TEOA $Co(bpy)_3^{2+}$	$MeCN/H_2O$	CO H_2	1453 863	λ ≥ 420 nm	[11]

$ZnIn_2S_4$ nanorods	TEOA	$MeCN/H_2O$	CO CH_4	1.5 0.22	$\lambda \geq 800$ nm	[12]
$ZnIn_2S_4/TiO_2$ nanosheets	TEOA $Co(bpy)_3^{2+}$	$MeCN/H_2O$	CO H_2	4410 /	300 W Xe lamp	[13]
Phosphorus-doped $ZnIn_2S_4$	TEOA $Co(bpy)_3^{2+}$	$MeCN/H_2O$	CO H_2	476 /	$\lambda \geq 420$ nm	[14]
Yolk–shell $TiO_2@ZnIn_2S_4$	TEOA	MeCN	CO H_2	325.29 227.18	LED $\lambda = 420$ nm	[15]
Oxygen-doped $C_3N_4/ZnIn_2S_4$	TEOA $Co(bpy)_3^{2+}$	$MeCN/H_2O$	CO CH_4	188.4 1.18	$\lambda \geq 400$ nm	[16]
WO_3-TiO_2/Cu_2ZnSnS_4	/	H_2O	CO CH_4	15.37 1.69	$\lambda > 420$ nm	[17]
NH_2-UiO-66/$CdIn_2S_4$	/	H_2O	11.24	2.91	300 W Xe lamp	[18]
$Cd_{0.5}Zn_{0.5}S/CdIn_2S_4$	/	H_2O	CO CH_4	14.07 4.23	300 W Xe lamp	[19]
WQDs/$CdIn_2S_4$	/	H_2O	CO CH_4	8.20 1.60	300 W Xe lamp	[20]
$CuInS_2/C/TiO_2$	/	H_2O	CO CH_4	7.73 /	300 W Xe lamp	[21]
$TiO_2/CsPbBr_3$	/	$MeCN/H_2O$	CO H_2	9.02 0.66	300 W Xe lamp	[22]
Ag–TiO_2/TS-1	/	H_2O	CO CH_4	3.16 0.47	300 W Xe lamp	[23]
COP-P/TiO_2	/	H_2O	CO CH_4	5.70 0.26	300 W Xe lamp	[24]

References

[1] H. Wang, J. J. Cao, Y. J. Zhou, X. Wang, H. Huang, Y. Liu, M. W. Shao, Z. H. Kang, Carbon

dots modified $Ti_3C_2T_x$-based fibrous supercapacitor with photo-enhanced capacitance, Nano Res. 2021, 14, 3886-3892.

[2] G. L. Mo, L. X. Wang, J. H. Luo, Controlled thermal treatment of NH_2-MIL-125(Ti) for drastically enhanced photocatalytic reduction of Cr(VI), Sep. Purif. Technol. 2021, 277, 119643.

[3] G. Yang, D. Chen, H. Ding, J. Feng, J. Z. Zhang, Y. Zhu, S. Hamid, D. W. Bahnemann, Well-designed 3D $ZnIn_2S_4$ nanosheets/TiO_2 nanobelts as direct Z-scheme photocatalysts for CO_2 photoreduction into renewable hydrocarbon fuel with high efficiency, Appl. Catal. B 2017, 219, 611-618.

[4] C. Yang, Q. Li, Y. Xia, K. Lv, M. Li, Enhanced visible-light photocatalytic CO_2 reduction performance of $Znln_2S_4$ microspheres by using CeO_2 as cocatalyst, Appl. Surf. Sci. 2019, 464, 388-395.

[5] K. Wang, X. Li, N. Wang, Q. Shen, M. Liu, J. Zhou, N Li, Z-scheme core-shell meso-TiO_2@$ZnIn_2S_4$/Ti_3C_2 MXene enhances visible light-driven CO_2-to-CH_4 selectivity. Ind. Eng. Chem. Res 2021, 60, 8720-8732.

[6] Y. Zhang, Y. X. Wu, L. Wan, H. J. Ding, H. X. Li, X. Y. Wang, W. H. Zhang, Hollow core-shell Co_9S_8@$ZnIn_2S_4$/CdS nanoreactor for efficient photothermal effect and CO_2 photoreduction, Appl. Catal. B 2022, 311, 121255.

[7] G. P. Zhang, X. W. Zhu, D. Y. Chen, N. J. Li, Q. F. Xu, H. Li, J. H. He, H. Xu, J. M. Lu, Hierarchical Z-scheme g-C_3N_4/Au/$ZnIn_2S_4$ photocatalyst for highly enhanced visible-light photocatalytic nitric oxide removal and carbon dioxide conversion, Environ. Sci.: Nano 2020, 7, 676-687.

[8] Q. Han, L. Li, W. Gao, Y. Shen, L. Wang, Y. Zhang, X. Wang, Q. Shen, Y. Xiong, Y. Zhou, Z. Zou, Elegant construction of $ZnIn_2S_4$/$BiVO_4$ hierarchical heterostructures as direct Z-scheme photocatalysts for efficient CO_2 photoreduction, ACS Appl. Mater. Interfaces. 2021, 13, 15092-15100.

[9] T. T. Hou, N. C. Luo, Y. T. Cuic, J. M. Lu, L. Li, K. E. MacArthure, M. Heggene, R. Chen, F. T. Fan, W. M. Tian, S. Y. Jin, F. Wang, Selective reduction of CO_2 to CO under visible light by controlling coordination structures of CeO_x-S/$ZnIn_2S_4$ hybrid catalysts, Appl. Catal. B 2019, 245, 262-270.

[10] B. Pan, Y. Wu, B. Rhimi, J. N. Qin, Y. Huang, M. Z. Yuan, C. Y. Wang, Oxygen-doping of

$ZnIn_2S_4$ nanosheets towards boosted photocatalytic CO_2 reduction, J. Energy. Chem. 2021, 57, 1-9.

[11] K. H. Chen, X. W. Wang, Q. Y. Li, Y. N. Feng, F. F. Chen, Y. Yu, Spatial distribution of $ZnIn_2S_4$ nanosheets on g-C_3N_4 microtubes promotes photocatalytic CO_2 reduction, Chem. Eng. J. 2021, 418, 129476.

[12] M. S. Yu, X. Y. Lv, A. M. Idris, S. H. Li, S. H. Li, J. Q. Lin, H. Lin, J. Wang, Z. Q. Li, Upconversion nanoparticles coupled with hierarchical $ZnIn_2S_4$ nanorods as a near-infrared responsive photocatalyst for photocatalytic CO_2 reduction, J. Colloid Interface Sci. 2022, 612, 782-791.

[13] E. Kim, K. H. Do, J. M. Wang, Y. Hong, A. P. Rangappa, D. A. Reddy, D. P. Kumar, T. K. Kim, Construction of 1D TiO_2 nanotubes integrated ultrathin 2D $ZnIn_2S_4$ nanosheets heterostructure for highly efficient and selective photocatalytic CO_2 reduction, Appl. Surf. Sci. 2022, 587, 152895.

[14] J. N. Qin, Q. Zhao, Y. L. Zhao, Y. Wu, B. Pan, C. Y. Wang, Metal-free phosphorus-doped $ZnIn_2S_4$ nanosheets for enhanced photocatalytic CO_2 reduction, J. Phys. Chem. C 2021, 125, 23813-23820.

[15] P. She, B. Y. Guan, J. Y. Sheng, Y. Y. Qi, G. Y. Qiao, H. B Rui, G. Y. Lu, J. S. Qin, H. Rao, Bioinspired spike-like double yolk-shell structured TiO_2@$ZnIn_2S_4$ for efficient photocatalytic CO_2 reduction, Catal. Sci. Technol. 2022, 12, 1092-1099.

[16] K. Zhu, J. O. Yang, Q. Zeng, S. G. Meng, W. Teng, Y. H. Song, S. Tang, Y. J. Cui, Fabrication of hierarchical $ZnIn_2S_4$@CNO nanosheets for photocatalytic hydrogen production and CO_2 photoreduction, Chin. J. Catal. 2020,41, 454-463.

[17] A. Raza, H. Shen, A. Haidry, L. Sun, R. Liu, S. Cui, Studies of Z-scheme WO_3-TiO_2/Cu_2ZnSnS_4 ternary nanocomposite with enhanced CO_2 photoreduction under visible light irradiation, J. CO_2 Util. 2020, 37, 260-271.

[18] L. Hong, R. Guo, Z. Zhang, Y. Yuan, X. Ji, Z. Lin, W. Pan, Fabrication of porous octahedron-flowerlike microsphere NH_2-UiO-66/$CdIn_2S_4$ heterojunction photocatalyst for enhanced photocatalytic CO_2 reduction, J. CO_2 Util. 2021, 51, 101650.

[19] Y. Yuan, R. Guo, Z. Zhang, L. Hong, X. Ji, Z. Lin, W. Pan, $Cd_{0.5}Zn_{0.5}S$ quantum dot-modified $CdIn_2S_4$ nano-octahedron as the 0D/3D hybrid heterojunction for CO_2 photoreduction, Energy Fuels. 2021, 35, 13291-13303.

[20] Z. Zhang, Y. Cao, F. Zhang, W. Li, Y. Li, H. Yu, M. Wang, H. Yu, Tungsten oxide quantum

dots deposited onto ultrathin $CdIn_2S_4$ nanosheets for efficient S-scheme photocatalytic CO_2 reduction via cascade charge transfer, Chem. Eng. J. 2022, 428, 131218.

[21] W. Bi, L. Zhang, H. Jiang, C. Li, Y. Hu, Construction of $CuInS_2/C/TiO_2$ hierarchical tandem heterostructures with optimized CO_2 photoreduction under visible light, Chem. Eng. J. 2022, 433, 133679.

[22] F. Xu, K. Meng, B. Cheng, S. Wang, J. Xu, J. Yu, Unique S-scheme heterojunctions in self-assembled $TiO_2/CsPbBr_3$ hybrids for CO_2 photoreduction, Nat. Commun 2020, 11, 4613.

[23] Y. Sun, G. Li, Y. Gong, Z. Sun, H. Yao, X. Zhou, Ag and TiO_2 nanoparticles co-modified defective zeolite TS-1 for improved photocatalytic CO_2 reduction, J. Hazard. Mater. 2021, 403, 124019.

[24] Y. Zhang, G. Zhang, Y. Wang, Z. Ma, T. Yang, T. Zhang, Y. Zhang, In-situ synthesized porphyrin polymer/TiO_2 composites as high-performance Z-scheme photocatalysts for CO_2 conversion, J. Colloid. Interf. Sci. 2021, 596, 342-351.